Interdomain exchange and the flip-flop of cholesterol in ternary component lipid membranes and their effects on heterogeneous cholesterol diffusion

Eun Sub Song, Younghoon Oh, and Bong June Sung
Department of Chemistry, Sogang University, Seoul 04107, Republic of Korea

(Received 10 June 2021; revised 9 September 2021; accepted 17 September 2021; published 4 October 2021)

Cell membranes are heterogeneous with a variety of lipids, cholesterol, and proteins and are composed of domains of different compositions. Such heterogeneous environments make the transport of cholesterol complicated: cholesterol not only diffuses within a particular domain but also travels between domains. Cholesterol also flip-flops between upper and lower leaflets such that cholesterol may reside both within leaflets and in the central region between two leaflets. How the presence of multiple domains and the interdomain exchange of cholesterol would affect the cholesterol transport, however, remains elusive. In this study, therefore, we perform molecular dynamics simulations up to 100 μs for ternary component lipid membranes, which consist of saturated lipids (dipalmitoylphosphatidylcholine, DPPC), unsaturated lipids (dilinoleylphosphatidylcholine, DIPC), and cholesterol. The ternary component membranes in our simulations form two domains readily: DPPC and DIPC domains. We find that the diffusion of cholesterol molecules is much more heterogeneous and non-Gaussian than expected for binary component lipid membranes of lipids and cholesterol. The non-Gaussian parameter of the cholesterol molecules is about four times larger in the ternary component lipid membranes than in the binary component lipid membranes. Such non-Gaussian and heterogeneous transport of cholesterol arises from the interplay among the interdomain kinetics, the different diffusivity of cholesterol in different domains, and the flip-flop of cholesterol. This suggests that in cell membranes that consist of various domains and proteins, the cholesterol transport can be very heterogeneous. We also find that the mechanism of the interdomain exchange differs for different domains: cholesterol tends to exit the DIPC domain along the central region of the membrane for the DIPC-to-DPPC transition, while the cholesterol is likely to exit the DPPC domain within the membrane leaflet for the DPPC-to-DIPC transition. Also, the interdomain exchange kinetics of cholesterol for the DPPC-to-DIPC transition is up to 7.9 times slower than the DIPC-to-DPPC transition.

DOI: 10.1103/PhysRevE.104.044402

I. INTRODUCTION

Cell membranes are composed of various lipids, cholesterol, and proteins and are intrinsically heterogeneous [1–4]. Most mammalian cell membranes, for example, consist of cholesterol up to its mole fraction (x_{chol}) of 0.5 and domains of different compositions [5]. The types and the compositions of lipids and cholesterol play important roles in the domain formation (and hence the formation of lipid rafts) [2,6–15]. In heterogeneous cell membranes with various domains, the transport of cholesterol becomes complicated because cholesterol not only diffuses within a particular domain but also undergoes interdomain exchanges between domains. Cholesterol also flip-flops, which is known to facilitate the lateral transport of cholesterol [16,17]. The cholesterol transport affects the domain formation, thus the cell signaling [18,19] as well as the rate of various biological processes in membrane [20–22]. How the heterogeneous environment, the interdomain exchange, and the flip-flop of cholesterol would affect the cholesterol transport should be a topic of importance. In this work, therefore, we perform molecular dynamics simulations for ternary component lipid membranes with two different striped domains and investigate the cholesterol diffusion.

The degree of the order of lipid tails is critical to the lipid phases [6–9,23–26]. Marrink *et al.* [27,28] suggested that the strong preference of cholesterol for saturated lipids should lead to the formation of cholesterol-rich liquid ordered phase (L_o). On the other hand, unsaturated lipids are likely to form a cholesterol-poor liquid disordered phase (L_d) with a small amount of cholesterol. The degree of the order of lipid tails also influences the self-diffusion and the flip-flop of cholesterol. The cholesterol in unsaturated lipid membranes flip-flops much faster than in saturated lipid membranes for a given value of x_{chol} [17,24]. Saturated lipid membranes are usually packed more tightly due to ordered lipid tails than unsaturated lipid membranes such that cholesterol has to overcome a larger free energy barrier to flip-flop, thus slowing the flip-flop kinetics in saturated membranes [29–34]. Similarly, the self-diffusion of cholesterol is slower in saturated lipid membranes for a given value of x_{chol} than in unsaturated lipid membranes [16,17].

The flip-flop of cholesterol plays an important role in domain registration between upper and lower leaflets [20,35]. In order for cholesterol to flip-flop from one leaflet to the other leaflet, cholesterol has to overcome a free energy barrier that arises from electrostatic interaction with neighbor lipids [33,34]. Before a flip-flop occurs, cholesterol lies with

canonical upright orientation within leaflets such that the hydrophilic head group of cholesterol can be placed around the membrane surface and the hydrophobic tail of cholesterol can be surrounded by lipid tails. In order for the cholesterol to flip-flop between leaflets, the cholesterol has to tilt down to the central region of the membrane between two leaflets and stay horizontal in between two leaflets. When x_{chol} increases, lipids become packed due to the condensing effect of cholesterol such that the flip-flop rate of cholesterol slows down.

The central region between two leaflets of bilayers (where cholesterol lies parallel during the flip-flop process) has often been considered as an unstable transition state for the flip-flop process. Previous studies suggested that both the number of double bonds in the lipid tails and the thickness of bilayers influences the presence of cholesterol in the central region [17,33,36–39]. When the tail group of a lipid is either less saturated or shorter, more cholesterol molecules can be found in the central region. On the other hand, for highly saturated and long lipids, a smaller amount of cholesterol can be placed in the central region, but the central region sometimes becomes a metastable state. The cholesterol at the metastable central region (between two leaflets of bilayers) diffuses up to eight times faster than within leaflets [16,40] such that cholesterol diffuses with two different diffusion coefficients depending on the spatial arrangement of the cholesterol [41–43].

In this work, we perform molecular dynamics simulations up to 100 μs for ternary mixtures of saturated lipids (DPPC), unsaturated lipids (DIPC), and cholesterol to investigate the effects of the interdomain exchange and flip-flop on the cholesterol diffusion. In our simulations, the ternary mixtures form two striped domains (DPPC-rich and DIPC-rich domains) for all values of x_{chol} from 0.13 to 0.3. As expected, we find that cholesterol in our simulations prefers the DPPC domain to the DIPC domain. In addition, both the diffusion coefficient and the flip-flop rate of cholesterol are higher in the DIPC domain than in the DPPC domain, mostly because DIPC lipids are less packed than DPPC lipids. Interestingly, the interdomain exchange kinetics of cholesterol for the DPPC-to-DIPC transition is at least five times slower than for the DIPC-to-DPPC transition. The mechanism of the interdomain exchange is also strongly dependent on the domain. For the DPPC-to-DIPC transition, cholesterol usually exits the DPPC domain and reaches the domain boundary by diffusing within leaflets. On the other hand, for the DIPC-to-DPPC transition, cholesterol diffuses through the central region (between two leaflets of bilayers) to exit the DIPC domain. This is attributed to the observation that more cholesterol molecules are found in the central region for unsaturated lipid membranes. The interdomain exchange process enhances the heterogeneity of the cholesterol diffusion. Compared to the binary component membranes (of both DPPC-cholesterol mixtures and DIPC-cholesterol mixtures) where the interdomain exchange is absent, the non-Gaussian parameter of cholesterol in the ternary component membranes is very large, indicating that cholesterol diffusion becomes very complicated and spatially heterogeneous due to the interdomain exchange.

The rest of this paper is organized as follows. In Sec. II we discuss our simulation model and methods in detail.

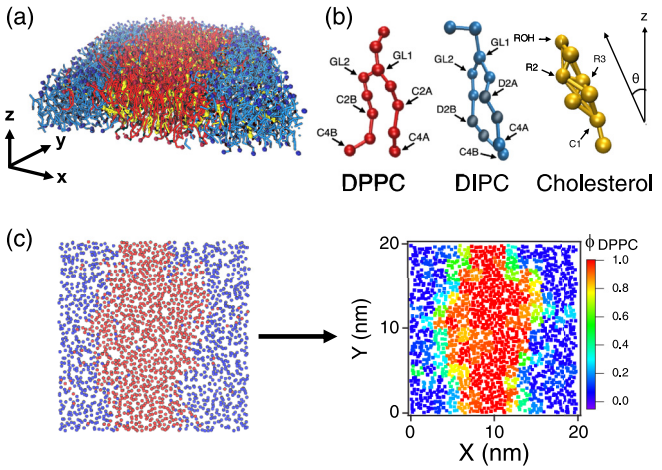

FIG. 1. (a) A representative simulation snapshot for $x_{\text{chol}} = 0.2$. Red, blue, and yellow molecules represent DPPC, DIPC, and cholesterol, respectively. (b) The molecular structures for the MARTINI model of DPPC, DIPC, and cholesterol with labels for beads and the definition of orientational angle θ. (c) A representative simulation snapshot (left) (projected on the xy-plane). The DPPC- and DIPC-domains are identified in the figure (right) with values of the local fraction (ϕ_{DPPC}). Red, blue, and green domains represent the DPPC, DIPC, and boundary domains, respectively.

Simulation results are discussed in Sec. III. Section IV contains the summary and conclusions.

II. MODEL AND METHODS

A. Model and simulation methods

We investigate ternary component lipid membranes composed of saturated lipids (dipalmitoylphosphatidylcholine, DPPC), unsaturated lipids (dilinoleylphosphatidylcholine, DIPC) and cholesterol at a temperature (T) of 330 K (Fig. 1). While the amounts of DPPC and DIPC lipids are kept equimolar, we tune the mole fraction (x_{chol}) of cholesterol from 0.13 to 0.3. We choose two types of lipids (DPPC and DIPC lipids) in this study because previous studies showed that the ternary mixtures of DPPC, DIPC, and cholesterol formed large striped domains of DPPC and DIPC lipids well [28]. The phase diagram of the ternary mixtures of DPPC, DIPC, and cholesterol was investigated systematically [44].

The initial configurations of ternary lipid membranes are constructed using the *insane* python script [45]. About 1350 lipids and cholesterol molecules are introduced into the ternary lipid membranes along with 15% of NaCl outside the lipid bilayers. The lateral dimension (L) of the simulation cell varies from 19 to 21 nm depending on x_{chol}. In order to compare with the ternary membranes, we also prepare the binary component lipid bilayers of both DPPC-cholesterol mixtures and DIPC-cholesterol mixtures with $L = 12$ nm, $T = 330$ K and 15% of NaCl. For simulation systems of both ternary and binary component bilayers, the dimension of the simulation cell in the z-direction (orthogonal to the membrane surface) is 15 nm.

We employ Dry MARTINI force fields [46–50] to simulate the ternary component lipid membranes. Note that all our

simulations are performed for the liquid phase of membranes because we aim in this study to investigate the effects of the interdomain exchange and the flip-flop on the cholesterol transport. Previous simulation studies showed that when a Dry MARTINI force field was employed, the melting temperature (T_M) of DPPC binary membranes of $x_{\rm chol} = 0.1$ was about 325 K [16]. Also, it is known that T_M decreases for the mixtures of DPPC lipids and unsaturated lipids [44,51]. The ternary component membranes of $T = 330$ K in this study, therefore, corresponds to the liquid phase.

We perform coarse-grained molecular dynamics simulations by employing Gromacs 2019 molecular simulation software [52–54]. In order to propagate our systems, we employ the second-order stochastic dynamics integrator with a time step of 30 fs for ternary membranes and 20 fs for binary membranes, and record trajectories every 30 ps to monitor the interdomain exchange of cholesterol [55–57]. All of the simulations in this work are performed under a semi-isotropic NpT ensemble to mimic tensionless lipid membranes. We also monitor and correct the motion of centers of mass of lipid molecules in upper and lower leaflet separately [58–60]. We equilibrate simulation systems over several hundreds of nanoseconds until the potential energy converges. We use a Berendsen barostat [61] during equilibration but employ a Parrinello-Rahman barostat [62] during the production run, which is as long as 100 μs for ternary lipid membrane systems and 50 μs for binary lipid membrane systems. The ensemble averages of properties are obtained over up to 10 different sets of trajectories for each state point.

B. Domains and structure of membranes

In our study, the ternary membranes (of equimolar DIPC and DPPC lipids, and cholesterol of $x_{\rm chol} = 0.13$ to 0.3) form coexisting striped domains readily. As shown in Fig. 1(a) and will be discussed in the next section, the ternary membranes in our study are composed of DPPC-rich (red) and DIPC-rich (blue) domains. Cholesterol molecules are more likely to be in the DPPC domain than in the DIPC domain. In order to identify the domains from the trajectories, we divide the simulation cell in lateral directions (xy-plane) into 196 boxes and calculate the local lipid fraction ($\phi_{\rm DPPC}$) of DPPC lipids for each box, i.e., $\phi_{\rm DPPC} = \frac{N_{\rm DPPC}}{N_{\rm DPPC}+N_{\rm DIPC}}$. Here $N_{\rm DPPC}$ and $N_{\rm DIPC}$ are the number of DPPC and DIPC lipids, respectively, in each box. If $\phi_{\rm DPPC} \approx 1$ (or 0), the box is composed of almost purely DPPC (or DIPC) lipids (not considering the presence of cholesterol) and corresponds to DPPC (or DIPC) domains. Figure 1(c) depicts a representative case for the identification of domains where the DPPC and the DIPC domains are clearly identified with $\phi_{\rm DPPC} \approx 1$ and 0, respectively. In the boundary between two domains, $\phi_{\rm DPPC} \approx 0.5$.

We also estimate the area per molecule (A_M) for each domain as follows. The areas ($A_{\rm box} = L^2/196$) of all 196 boxes are identical but ranges from 1.8 nm^2 to 2.2 nm^2 depending on $x_{\rm chol}$ and the number of molecules in the simulation cell. We count the number ($M_{\rm DPPC}$) of boxes (out of total 196 boxes) with $\phi_{\rm DPPC} \approx 1$ and the number $N_{T,\rm DPPC}$ of all molecules (including cholesterol) in those boxes. Then A_M for the DPPC domain is $A_M = \frac{A_{\rm box} M_{\rm DPPC}}{N_{T,\rm DPPC}}$. A_M for the DIPC domain can be obtained similarly, i.e., $A_M = \frac{A_{\rm box} M_{\rm DIPC}}{N_{T,\rm DIPC}}$, where $M_{\rm DIPC}$ and $N_{T,\rm DIPC}$ are the number of boxes with $\phi_{\rm DPPC} \approx 0$ and the number of all molecules in those boxes, respectively. We monitor the local mole fraction of cholesterol ($x_{\rm local}$) for each particular domain. That is to say, $x_{\rm local}$ in the DPPC domain is calculated by using $x_{\rm local} = \frac{N_{\rm CHOL,DPPC}}{N_{T,\rm DPPC}}$, where $N_{CHOL,\rm DPPC}$ and $N_{T,\rm DPPC}$ are the numbers of cholesterol in the DPPC domain and the total number of molecules in the DPPC domain, respectively. We also calculate the order parameter for cholesterol molecules in each domain by using $P_2 \equiv \frac{1}{2}(3\langle\cos^2\beta\rangle - 1)$. β denotes the angle of the second lipid tail segment with respect to the vector normal to the membrane surface. If $P_2 \approx 1$, the lipid tails are ordered and stretched out normal to the membrane surface.

The Dry MARTINI force field is an implicit solvent model and allows us to investigate the cholesterol transport at long-time scales as long as 100 μs. In order to verify the validity of the Dry MARTINI force field, we compare our results with a previous simulation study for ternary component membranes [44] that employed the Wet MARTINI force field. We calculate (1) the number (%Chol contacts) of contacts between cholesterol and lipids as the percentage of total lipid-lipid contacts, (2) the mixing entropy, (3) the contact numbers of both intraleaflet and interleaflet, (4) P_2 order parameter for the structure of lipid tails, and (5) the hexatic order parameter (ψ_6) as shown in Fig. 2.

As shown in Figs. 2(a) and 2(b), we calculate %Chol-lipid contacts and the binary lateral mixing entropy ($S_{\rm mix}$). The %Chol-lipid contact is monitored as the percentage of all DPPC-cholesterol (DIPC-cholesterol) contacts out of all DPPC-lipid (DIPC-lipid) contacts. $S_{\rm mix}$ is evaluated by counting the numbers of DPPC-DPPC, DIPC-DIPC, and DPPC-DIPC headgroups with nearest neighbors determined with Voronoi tessellation. In order to investigate the phase separation of membranes quantitatively, we also monitor transleaflet clustering as shown in Figs. 2(c) and 2(d). The domain sizes of DPPC and cholesterol is evaluated by counting both the contact numbers of intra- (n) and interleaflet (m). n indicates the number of beads within a separated domain in each leaflet. On the other hand, m represents the number of beads within one cluster in opposite leaflets. Cutoff distances are used to calculate the contact numbers of n and m in each cluster. If a distance between two arbitrary beads is less than the cutoff, we determine that two beads belong to one cluster. Cutoff distances are 5.8 Å and 7.0 Å for the contact number n and m, respectively. C2A or C2B bead of DPPC molecules and the center of a cholesterol molecule are used to characterize the contact number n. C4A or C4B bead of DPPC molecules and C2 bead of a cholesterol molecule are used to calculate the contact number m. As shown in Figs. 2(d) and 2(f), we calculate structure of membrane molecules with order parameters, P_2 and $\langle\Psi_6\rangle$, regardless of their domain. The order parameter, P_2, is estimated by using the vector from GL1 (GL2) to C4A (C4B) beads of lipid molecules and the vector normal to the membrane surface. In order to monitor the lateral packing of membrane molecules in each leaflet, we calculate the hexatic order parameter, $\langle\Psi_6\rangle \equiv \langle\frac{1}{6}\sum_{l=1}^{6}\exp(-i6\theta_{kl})\rangle$. C2A or C2B beads of DPPC lipids, D2A or D2B of DIPC lipids, and the center of mass of cholesterol molecules are used to calculate $\langle\Psi_6\rangle$. We pick one

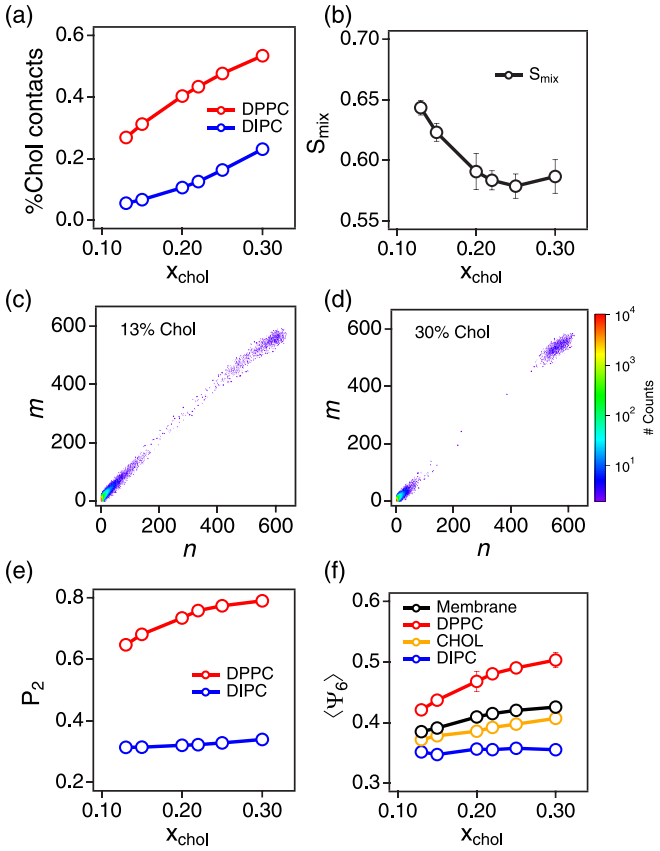

FIG. 2. (a) Number of cholesterol-lipid contacts with DPPC and DIPC as the percentage of total lipid-lipid contacts. (b) The lateral binary mixing entropy ($S_{\rm mix}$) for ternary lipid membranes. Occurrences of intra- (n) and interleaflet (m) lipid tails in trans-leaflet DPPC-cholesterol domains (c) for 13% cholesterol and (d) for 30% cholesterol. (e) P_2 order parameter and (f) for the hexatic order parameter ($\langle\Psi_6\rangle$) as functions of $x_{\rm chol}$.

bead (the kth bead) and its six nearest beads (the lth bead), and search for the best plane of those beads to measure θ_{kl}. Here θ_{kl} denotes the angle between an arbitrary reference vector on the plane and a bond vector of the kth to the lth bead. If $\langle\Psi_6\rangle \approx 1$, the membrane molecules are packed ideally.

%Chol-lipid contacts, $S_{\rm mix}$ and the contact numbers of intra- (n) and interleaflet (m) from our simulations are similar to those from the previous study [44], which indicates that the coarse-grained model with the Dry MARTINI force field can be a good model for the membrane phase separations. On the other hand, the structure of membrane molecules are slightly different from the previous study as shown in Figs. 2(d) and 2(f). Both P_2 and $\langle\Psi_6\rangle$ in our study are smaller than values from the previous study. This is consistent with a previous study by Stelter *et al.* that employed both Wet and Dry MARTINI force fields for DPPC binary lipid membranes and compared P_2 order parameters [63].

C. The diffusion and the kinetics in membranes

In order to investigate the lateral diffusion of molecules, we calculate the lateral mean-squared displacement $[\langle(\Delta r)^2(t)\rangle \equiv \langle[\vec{r}_i(t) - \vec{r}_i(0)]^2\rangle]$ of each component in ternary lipid membranes. In case of DPPC or DIPC lipids, $\vec{r}_i(t)$ is the position vector of the second tail bead of the ith lipid (C2A and C2B for DPPC lipids or D2A and D2B for DIPC lipids) at time t projected onto the xy-plane (the membrane surface) [Fig, 1(b)]. In case of cholesterol, $\vec{r}_i(t)$ denotes the ring bead of the ith cholesterol (R2 and R3) at time t projected onto the xy-plane [Fig. 1(b)]. We assume that the undulation of the lipid membrane might be negligible. $\langle\cdots\rangle$ denotes an ensemble average. We employ the Einstein's relation $[\lim_{t\to\infty}\langle(\Delta r)^2(t)\rangle = 4Dt]$ to estimate the lateral diffusion coefficient (D) of each component [64–66]. The non-Gaussian parameter $[\alpha_2(t) \equiv \frac{\langle(\Delta r)^4(t)\rangle}{2\langle(\Delta r)^2(t)\rangle^2} - 1]$ is employed to measure how much the diffusion of each component deviates from being Gaussian. We also monitor the self-part of the van Hove correlation function $[G_s(r,t) \equiv \langle\delta\{r - |\vec{r}_i(t) - \vec{r}_i(t=0)|\}\rangle]$ for each component [17,67,68].

In order to take a track of the flip-flop events of the cholesterol, we investigate the z position of ROH bead and the angle (θ) between the vector from C1 bead to ROH bead and the vector normal to the membrane surface [Fig. 1(b)]. We categorize cholesterol into *the center cholesterol* and *the leaflet cholesterol* by calculating θ and the value ($z_{\rm ROH}$) of the z-coordinate of the ROH bead of the cholesterol. If $|z_{\rm ROH}| \leqslant 0.5$ nm and $70^\circ < \theta < 110^\circ$, the cholesterol is located at the central region in between two leaflets and is categorized as the center cholesterol. On the other hand, cholesterol molecules with $|z_{\rm ROH}| \geqslant 1.5$ nm and $\theta > 165^\circ$ or $\theta < 15^\circ$ are categorized into the leaflet cholesterol. In the case where cholesterol changes from upper leaflet to lower leaflet (or lower leaflet to upper leaflet), we decide that the cholesterol should undergo a flip-flop.

We calculate the first passage time ($\tau_{\rm inter}$) taken for a cholesterol molecule to travel from one domain and arrive at the boundary between two domains. For example, consider a cholesterol molecule in a box of $\phi_{\rm DPPC} \approx 1$, which travels and reaches the boundary of $\phi_{\rm DPPC} \approx 0.5$. The time taken for the cholesterol molecule to travel is considered as a first passage time for the DPPC-to-DIPC interdomain exchange. We also calculate the rate (γ) of flip-flop process by calculating the number of flip-fop events that occur for cholesterol within each domain during a unit time.

III. RESULTS AND DISCUSSION

A. The domains and structure of ternary membranes

The binary mixtures of DIPC lipids and cholesterol usually form single L_d phases even at high cholesterol concentration. On the other hand, the binary mixtures of DPPC lipids and cholesterol begin to form coexistent liquid ordered (L_o) and liquid disordered (L_d) phases at $x_{\rm chol} = 0.1$, and form single L_o phases beyond $x_{\rm chol} \approx 0.2$ [69]. Ternary mixtures of cholesterol and saturated and unsaturated lipids may form coexistent L_o and L_d phases depending on the temperature and the composition [23–25,44,70–73]. For example, Pantelopulos *et al.* showed that ternary lipid membranes of cholesterol, DPPC, and DIPC lipids form striped separated domains for $x_{\rm chol}$ from 0.1 to 0.4 [44]. The ternary membranes in our simulations also form striped domains of DPPC-rich and DIPC-rich phases for $x_{\rm chol}$ from 0.1 to 0.3 [Fig. 1(a)], which is consistent with previous studies.

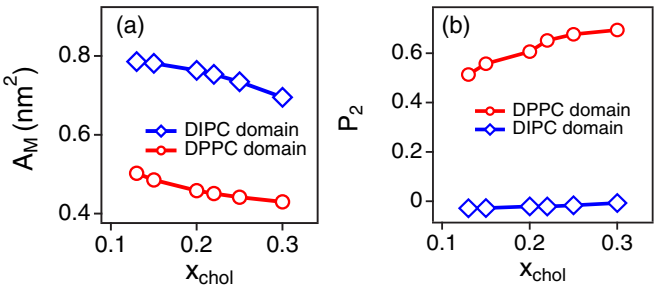

FIG. 3. (a) The local area per molecule (A_M) as a function of x_{chol} for DPPC (red) and DIPC (blue) domains. (b) The order parameter (P_2) of lipids as a function of x_{chol} for DPPC (red) and DIPC (blue) domains.

As expected from previous studies, the DPPC domain is packed more significantly than the DIPC domain. Figure 3(a) depicts the local area per molecule (A_M) as a function of x_{chol}. For a relatively small fraction (x_{chol}) of 0.1, A_M of the DPPC domain is small around 0.5 nm^2 while $A_M \approx 0.8$ nm^2 for the DIPC domain. As more cholesterol molecules are introduced into the membrane, A_M decreases, thus indicating that molecules are packed more efficiently due to the condensing effect of cholesterol. The difference in A_M between DPPC and DIPC domains is attributed to the degree of order of lipid tails. As shown in Fig. 3(b), the order parameter (P_2) of DIPC lipids in DIPC domains is much smaller than that of DPPC lipids in DPPC domains: $P_2 \approx 0$ for DIPC lipids while P_2 for DPPC lipids range from 0.5 to 0.7.

B. The spatial arrangement and the flip-flop of cholesterol

Cholesterol molecules prefer DPPC domains to DIPC domains. Figure 4(a) depicts the local mole fractions (x_{local}) of cholesterol in both DPPC and DIPC domains as a function of the overall mole fraction (x_{chol}). x_{local} for both DPPC and DIPC domains increase with an increase in x_{chol} because more cholesterol molecules are introduced into systems. But x_{local} is much larger for DPPC domains than for DIPC domains. Even for $x_{chol} = 0.3$ where the amount of cholesterol in the DIPC domain is the largest in our study, x_{local} for the DPPC domain is about three times larger than for the DIPC domain.

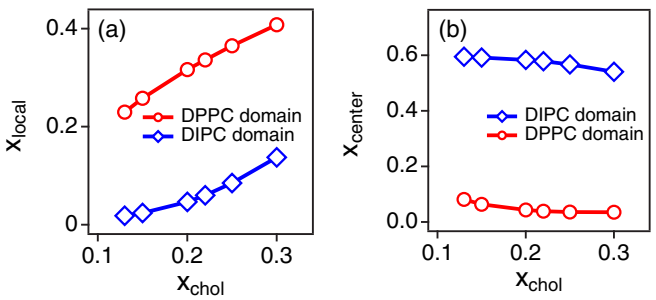

FIG. 4. (a) The local mole fraction (x_{local}) of cholesterol as a function of x_{chol} for DPPC (red) and DIPC (blue) domains. (b) The fraction (x_{center}) of cholesterol in the central region between two leaflets as a function of x_{chol} for DPPC (red) and DIPC (blue) domains.

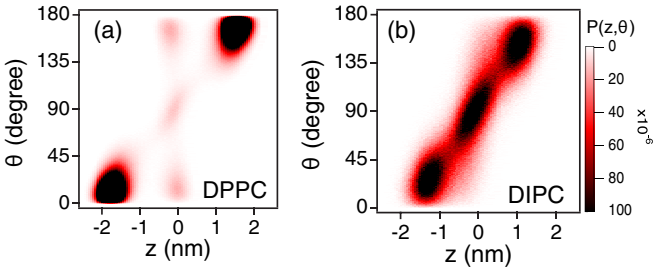

FIG. 5. The probability density function ($P(z, \theta)$) of cholesterol at $x_{chol} = 0.2$ (a) for the DPPC domain and (b) for the DIPC domain.

Harroun *et al.* investigated cholesterol in unsaturated lipid membrane by performing neutron diffraction experiments, and showed that cholesterol could reside in the central region between two leaflets [74]. Marrink *et al.* also showed in their simulations that cholesterol preferred the central region between two leaflets in unsaturated lipid membranes. [75] As more unsaturated tail beads were introduced, cholesterol tended to reside in the central region [17,40]. In our simulations, more than half of cholesterol molecules in the DIPC domain are located at the central region between two leaflets even at $x_{chol} = 0.30$ [Fig. 4(b)]. On the other hand, most of cholesterol molecules in the DPPC domain are located within leaflets with canonical upright orientations. We calculate the fraction (x_{center}) of cholesterol molecules located in the central region within a given domain. Therefore, x_{center} is the ratio of cholesterol molecules in the central region to the total number of cholesterol molecules in the domain. As shown in Fig. 4(b), x_{center} in DIPC domains is always larger than 0.5, even though x_{center} decreases with an increase in x_{local}. On the other hand, $x_{center} < 0.1$ in the DPPC domain, thus indicating that less than 10% of cholesterol molecules in the DPPC domain are likely to be in the central region and most cholesterol molecules are within two leaflets.

We investigate the probability density function ($P(z, \theta)$) of cholesterol in both DPPC and DIPC domains (Fig. 5) [76]. Here z denotes the position of the R2 and R3 beads of cholesterol molecules in the direction (z-axis) normal to the membrane surface. θ is an angle between the vector from the C1 bead of cholesterol to the ROH bead and the unit vector along the z-axis [Fig. 1(b)]. Note that $\theta = 0^\circ$ and 180° correspond to cholesterol with canonical upright orientations, whereas $\theta \approx 90^\circ$ is for cholesterol staying parallel to the membrane surface. The peaks at $(z, \theta) \approx (0, 90^\circ)$ of $P(z, \theta)$ indicate that some cholesterol molecules stay in the central region while others stay within the membrane leaflets with $(z, \theta) \approx (2\text{ nm}, 180^\circ)$ or $(-2\text{ nm}, 0^\circ)$. As shown in Fig. 5(b), $P(z, \theta)$ has a large peak at $(z, \theta) \approx (0, 90^\circ)$, thus suggesting that cholesterol molecules in the DIPC domain are more likely to be in the central region between two leaflets than in the DPPC domain.

We estimate the restricted free energy profile $[F(z)]$ of cholesterol as a function of z by using $F(z) \equiv -k_B T \ln[\int_{\theta=0}^{\pi} P(z, \theta) d\theta]$ [77]. Here k_B denotes the Boltzmann constant. Figures 6(a) and 6(b) represent $F(z)$ for DIPC and DPPC domains, respectively, at $x_{chol} = 0.2$. The free energy difference (ΔF_γ) between the leaflet and the center states is

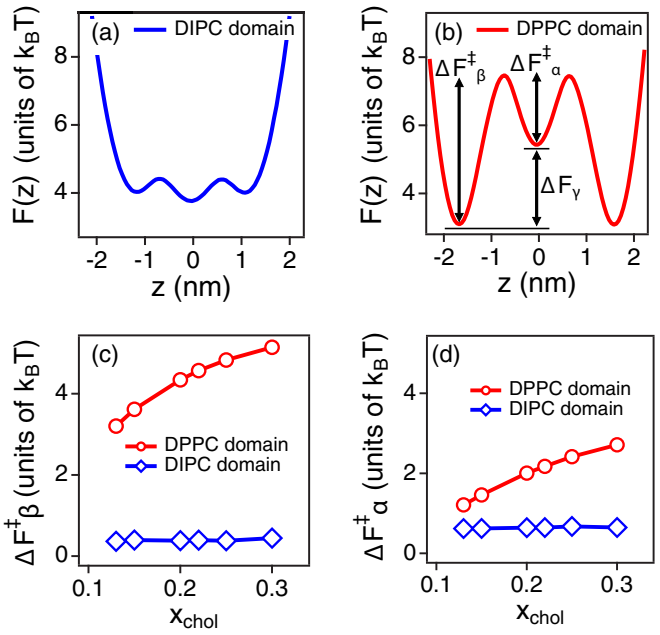

FIG. 6. The restricted free energy profiles ($F(z)$) in (a) the DIPC domain and (b) the DPPC domain at $x_{\rm chol} = 0.2$. See the discussion for $\Delta F_\alpha^\ddagger$, $\Delta F_\beta^\ddagger$, and ΔF_γ. (c) $\Delta F_\beta^\ddagger$ as a function of $x_{\rm chol}$ for the DPPC and DIPC domains. (d) $\Delta F_\alpha^\ddagger$ as a function of $x_{\rm chol}$ for the DPPC and DIPC domains.

smaller in the DIPC domain than in the DPPC domain. Therefore, a relatively large amount of cholesterol can be found in the central region in DIPC domains with a large $x_{\rm center}$. In DPPC domains, however, $x_{\rm center}$ is relatively small and most cholesterol molecules stay within leaflets.

We also investigate the free energy barrier ($\Delta F_\beta^\ddagger$) for the cholesterol molecule to travel from the leaflet state to the center state [Fig. 6(c)]. $\Delta F_\beta^\ddagger$ determines how quickly the cholesterol molecule flip-flops. $\Delta F_\beta^\ddagger$ is much larger in the DPPC domain than in the DIPC domain by more than an order of magnitude. This suggests that the flip-flop of cholesterol in the DIPC domain should be much faster than in the DPPC domain [17]. Javanainen *et al.* suggested that the free energy barrier for flip-flops decreased by ~1.6 kJ/mol ($\approx 0.5 k_B T$) per double bond at the same $x_{\rm chol}$ [40], which indicates that it would be much easier for cholesterol in unsaturated lipid membranes to flip-flop. This is consistent with our result that $\Delta F_\beta^\ddagger$ difference between in DPPC domain and DIPC domain is at least 2.5 k_BT.

We also count the number of flip-flop events per unit time and calculate the flip-flop rate (γ) for cholesterol molecules in both DIPC and DPPC domains (Fig. 7). As expected from the results for $\Delta F_\beta^\ddagger$, γ of cholesterol in the DIPC domain is faster by an order of magnitude than in the DPPC domain. γ decreases with an increase in $x_{\rm chol}$, which is also consistent with an increase in $\Delta F_\beta^\ddagger$ [Fig. 6(c)]. Gu *et al.* simulated ternary membranes with DPPC, DOPC, and cholesterol, and calculated DOPC enrichment by estimating the ratio of the concentration of DOPC around cholesterol to the average concentration of DOPC [71]. For example, if DOPC enrichment were to be zero, the cholesterol resides in DPPC

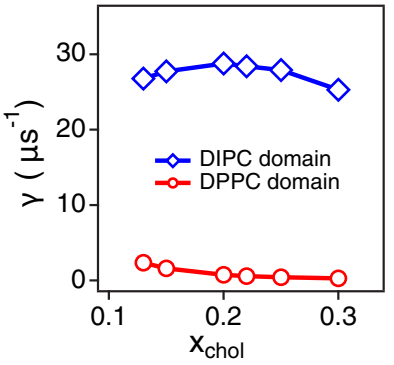

FIG. 7. The simulation results for the flip-flop rate (γ) of cholesterol in the DPPC and DIPC domains.

environment. They also monitored the flip-flop rates for a given DOPC enrichment and proposed that the flip-flop rate in the lowest DOPC enrichment was seven times slower than in the highest DOPC enrichment, which is consistent with our result.

$\Delta F_\alpha^\ddagger$ quantifies how metastable the center state of cholesterol would be [Fig. 6(d)]. We find that in case of cholesterol in the DPPC domain, $\Delta F_\alpha^\ddagger$ becomes larger than a thermal energy ($k_B T$) such that cholesterol may stay at the center state for relatively long times even if $x_{\rm local}$ is small for the DPPC domain.

We divide the simulation cell in lateral directions into 196 boxes and calculate the local lipid fraction ($\phi_{\rm DPPC}$) of DPPC lipids for each box. We monitor γ, P_2, and A_M for each box. Not surprisingly, the area (A_M) per molecule decreases gradually from $\phi_{\rm DPPC} = 0$ to $\phi_{\rm DPPC} = 1$ (or DIPC domain to DPPC domain). P_2 for both DPPC molecules and DIPC molecules gradually increase from $\phi_{\rm DPPC} = 0$ to $\phi_{\rm DPPC} = 1$. At the same time, the flip-flop rate (γ) of cholesterol decreases from $\phi_{\rm DPPC} = 0$ to $\phi_{\rm DPPC} = 1$. This suggests that γ, A_M, and P_2 should relate to one another. For example, cholesterol molecules experience a larger free energy barrier for the flip-flop process when either A_M is low or P_2 is higher.

C. The lateral diffusion of cholesterol

The lateral diffusion of cholesterol is subject to quite spatially heterogeneous environments due to the presence of two domains [58,68,78–80]. At a given temperature T, the diffusion of DPPC lipids is much slower than that of DIPC lipids. Figure 8(a) depicts the self-diffusion coefficient (D) of each component as a function of $x_{\rm chol}$. D of DIPC lipids is larger by a factor of up to 4 than that of DPPC lipids. The diffusion of DIPC lipids is less heterogeneous than that of DPPC lipids such that the non-Gaussian parameter [$\alpha_2(t)$] of DIPC lipids is much small compared to that of DPPC lipids. Figure 8(b) shows $\alpha_2(t)$ of DPPC lipids where $\alpha_2(t)$ of DPPC lipids increases up to about 1 at $x_{\rm chol} = 0.3$ and $t \approx 200$ ns.

The lateral diffusion of cholesterol is faster than DPPC lipids but slower than DIPC lipids [Fig. 8(a)]. The cholesterol diffusion is, however, the most heterogeneous than any other component in our membranes. As shown in Fig. 8(c), $\alpha_2(t)$ of cholesterol is much larger than that of any other lipids. $\alpha_2(t)$ reaches its maximum value ($\alpha_{2,\rm max}$) before $t \approx 40$ ns such

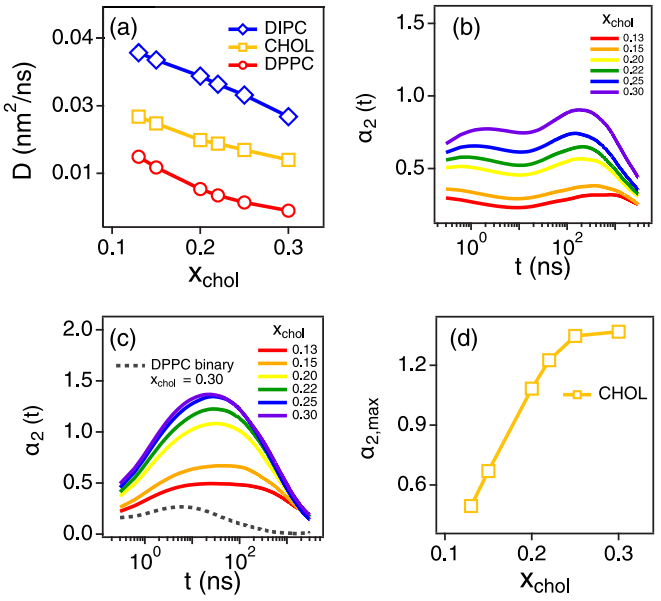

FIG. 8. (a) The lateral diffusion coefficients (D) of each components in ternary lipid membranes. (b) The non-Gaussian parameter [$\alpha_2(t)$] of DPPC lipids for different values of $x_{\rm chol}$. (c) $\alpha_2(t)$ of cholesterol for different values of $x_{\rm chol}$. Note that a dashed line in the figure corresponds to $\alpha_2(t)$ of cholesterol in the binary lipid membrane of DPPC lipids and cholesterol with $x_{\rm chol} = 0.3$. (d) The maximum value ($\alpha_{2,\rm max}$) of $\alpha_2(t)$ of cholesterol as a function of $x_{\rm chol}$.

that the cholesterol diffusion becomes heterogeneous at earlier times than the lipid diffusion. As more cholesterol molecules are introduced into the ternary membranes, D of all components decrease due to the condensing effect of cholesterol. Similarly, $\alpha_2(t)$ of both lipids and cholesterol are increased.

The lateral diffusion of cholesterol is more heterogeneous in the DPPC domain than in the DIPC domain. Figure 9 depicts the self-part of van Hove correlation function [$G_s(r,t)$] of cholesterol at $t = 6$ ns and 60 ns in both DPPC and DIPC domains with $x_{\rm chol} = 0.3$. In the DIPC domain, $G_s(r,t)$ at short and long times are Gaussian, which suggests that cholesterol molecules diffuse with a single diffusion coefficient and the lateral diffusion should be homogeneous. On the other hand, $G_s(r,t)$ of cholesterol in the DPPC domain deviate from being Gaussian at both long and short times. $G_s(r, t = 60$ ns) of cholesterol in the DPPC domain at $t = 60$ ns clearly shows that there are two sets of cholesterol: (1) some cholesterol

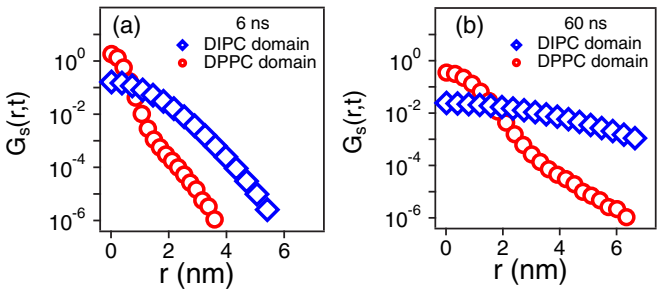

FIG. 9. The self-part of van Hove correlation functions ($G_s(r,t)$) of cholesterol in DPPC and DIPC domains at (a) $t = 6$ and (b) 60 ns.

molecules diffuse slowly within 2 nm at $t = 60$ ns and (2) other cholesterol molecules diffuse rapidly beyond 2 nm at the same time. This indicates that the lateral diffusion of cholesterol in the DPPC domain should be heterogeneous.

Such a heterogeneous cholesterol diffusion in the DPPC domain has to relate to the stability of the central region of membranes. $\Delta F_\alpha^\ddagger$ is much larger in the DPPC domain than in the DIPC domain, especially at $x_{\rm chol} = 0.3$ [Fig. 6(d)]. This makes the cholesterol molecule in the central region between two leaflets more stable in the DPPC domain. It has been well known that the cholesterol molecule in the central region should diffuse much faster than within leaflets [16,17,40,74,75,81]. Therefore, cholesterol molecules in the DPPC domain should diffuse with two different diffusivities depending on the spatial arrangement, which makes the cholesterol diffusion non-Gaussian and spatially heterogeneous.

Interesting is that the lateral diffusion of cholesterol is much more heterogeneous in the ternary membranes than in the binary membranes. A dashed line in Fig. 8(c) corresponds to $\alpha_2(t)$ of cholesterol in the binary membrane composed of DPPC lipids and cholesterol. Note that $x_{\rm chol} = 0.3$ for this binary membrane and $T = 330$ K. The maximum value ($\alpha_{2,\rm max}$) of $\alpha_2(t)$ is only about 0.3 for the binary membrane while $\alpha_{2,\rm max}$ reaches 1.4 for ternary membranes. In the binary membranes of DPPC lipids and cholesterol, the lateral diffusion of cholesterol is still slow (due to the high-order parameter of DPPC lipids and the condensing effect of cholesterol), and the cholesterol also flip-flops to some extent. A previous simulation study, therefore, shows that cholesterol diffusion in the DPPC lipid bilayers is spatially heterogeneous [16] to some extent. It is the interdomain exchange of cholesterol molecules that does not occur in the binary membranes but occurs readily in the ternary membranes. Therefore, it is the presence of the interdomain exchange of cholesterol (discussed in the next subsection) that enhances the non-Gaussianity of cholesterol diffusion.

D. The interdomain exchange of cholesterol

It takes a longer time for a cholesterol molecule to travel from the DPPC domain to the domain boundary between domains than from the DIPC domain to the domain boundary. We estimate the average first passage time ($\tau_{\rm inter}$) for both DPPC-to-DIPC and DIPC-to-DPPC transitions. As shown in Fig. 10(a), $\tau_{\rm inter}$ for the DPPC-to-DIPC transition is up to 7.9 times larger than for the DIPC-to-DPPC transition. Such a slow interdomain exchange for the DPPC-to-DIPC transition is attributed to two factors: (1) the strong preference of cholesterol for the DPPC domain and (2) the slow diffusion of cholesterol in DPPC domains.

As shown in Fig. 4(a), the local mole fraction ($x_{\rm local}$) of cholesterol is much larger in the DPPC domain than in the DIPC domain. For example, for the overall mole fraction of $x_{\rm chol} = 0.3$, $x_{\rm local}$ is 2.9 times larger in the DPPC domain. This corresponds to the difference of about 1.1 k_BT in the Gibbs free energy of cholesterol and makes the activation energy of the DPPC-to-DIPC transition larger by 1.1 k_BT than that of the DIPC-to-DPPC transition.

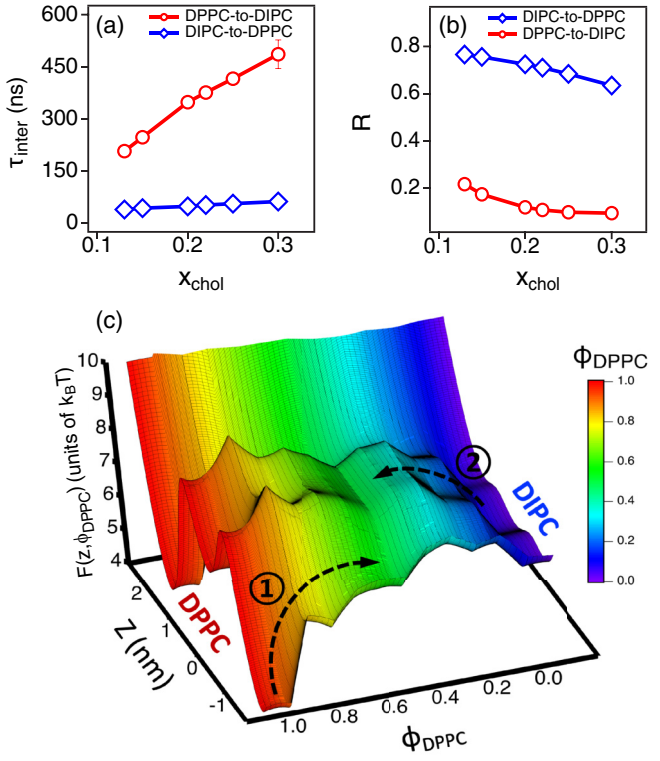

FIG. 10. (a) The first passage time (τ_{inter}) of cholesterol for both the DPPC-to-DIPC transition (red) and the DIPC-to-DPPC transition (blue). (b) The fraction (R) of cholesterol that exits the given domain in the central region and reaches the boundary between domains. (c) The restricted free energy profile $[F(z, \phi_{DPPC})]$ of cholesterol as a function of z and ϕ_{DPPC} at $x_{chol} = 0.30$. The color code represents ϕ_{DPPC} as in Fig. 1(c). Most cholesterol molecules in the DPPC domain undergo the DPPC-to-DIPC transition along path 1. On the other hand, most cholesterol molecules in the DIPC domain undergo the DIPC-to-DPPC transition along path 2.

In addition to the activation energy, the lateral diffusion of cholesterol is much slower in the DPPC domain than in the DIPC domain. It takes, therefore, much longer for cholesterol to sample in the phase space of the DPPC domain than in the DIPC domain. This also makes the kinetics of the DPPC-to-DIPC transition slow.

Not only the kinetics of the interdomain exchange but also the mechanism at a molecular level for the exchange depends on the domain. We find from our simulations that cholesterol in the DIPC domain travels from the DIPC domain to the boundary in the central region between two leaflets. On the other hand, cholesterol in the DPPC domain travels through leaflets to reach the boundary. Figure 10(b) depicts the fraction (R) of cholesterol molecules that leaves the given domain and reaches the boundary in the central region. $R \geqslant 0.6$ for the DIPC-to-DPPC transition while $R \leqslant 0.2$ for the DPPC-to-DIPC transition. This is attributed mostly to the fact that many cholesterol molecules are placed in the central region for the DIPC domain while a smaller fraction of cholesterol molecules stay in the central region for the DPPC domain.

We also estimate the restricted free energy profile $[F(z, \phi_{DPPC})]$ of cholesterol as a function of z and ϕ_{DPPC} by using $F(z, \phi_{DPPC}) \equiv -k_BT \ln[P(z, \phi_{DPPC})]$. Figure 10(c) depicts $F(z, \phi_{DPPC})$ for $x_{chol} = 0.3$. The restricted free energy profile $[F(z, \phi_{DPPC})]$ clearly shows how and why the interdomain exchange mechanism depends on the domains. When the cholesterol resides within the DIPC domain ($\phi_{DPPC} = 0$) initially, $F(z, \phi_{DPPC})$ is low at $z = 0$ such that the cholesterol travels to the transition state of $\phi_{DPPC} = 0.5$ along the central plane of the lipid bilayers (indicated by path 2 in Fig. 10(c)]. On the other hand, when the cholesterol resides within the DPPC domain ($\phi_{DPPC} = 1$) initially, $F(z, \phi_{DPPC})$ is low at $z = \pm 1$ nm such that most cholesterol has to stay within the leaflets. Therefore, most cholesterol molecules in DPPC domain undergo the DPPC-to-DIPC transition along path 1. Because the cholesterol in DPPC domain has to overcome much higher free energy barrier to travel to the transition state, the interdomain exchange kinetics of cholesterol for the DPPC-to-DIPC transition was up to 7.9 slower.

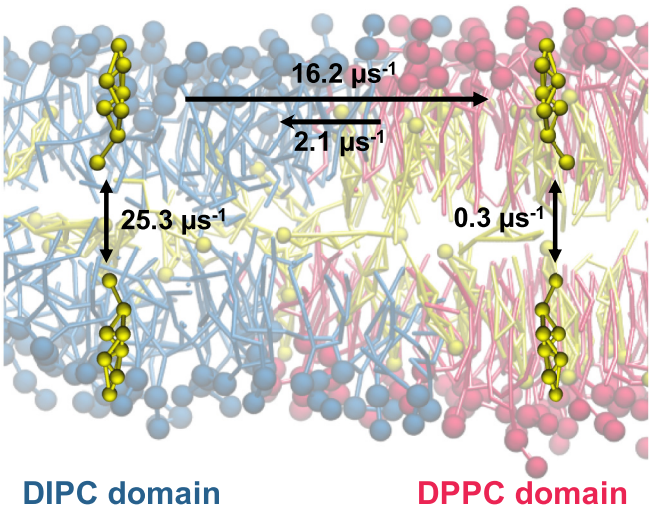

FIG. 11. A schematic for processes of cholesterol in the ternary membranes: the lateral diffusion, the flip-flop, and the interdomain exchange. The numbers indicate the rate of various processes for cholesterol molecules in ternary membranes at $x_{chol} = 0.3$.

IV. SUMMARY AND CONCLUSION

In this study, we perform extensive molecular dynamics simulations to investigate the effects of the presence of different domains in ternary membranes on the cholesterol transport. We also consider the effects of the flip-flop, the interdomain exchange, and the presence of metastable center states. Figure 11 summarizes the kinetics of various processes of cholesterol in the ternary membranes. Due to the presence of two different domains, flip-flop processes, the interdomain exchange, and the presence of the metastable central region, the cholesterol molecule is subject to a very heterogeneous environment. While the lateral diffusion of cholesterol in the DIPC domain is fast and homogeneous, the cholesterol in the DIPC domain undergoes both the flip-flop and the interdomain exchange relatively fast. The cholesterol molecule in the DPPC domain not only diffuses slowly but also flip-flops slowly due to the presence of a large free energy barrier ($\Delta F_\beta^\ddagger$). In addition, in the DPPC domain, $\Delta F_\alpha^\ddagger$ is also large

such that the central region becomes metastable for cholesterol, which makes the cholesterol diffusion heterogeneous. With the effects of all those processes together, the lateral diffusion of cholesterol becomes heterogeneous more significantly than in binary membranes.

ACKNOWLEDGMENTS

This work was supported by a National Research Foundation of Korea (NRF) grant funded by the Korean government (MSIT) (Grant No. 2019R1A2C2084053). This research was supported by the Basic Science Research Program through the National Research Foundation of Korea (NRF) funded by the Ministry of Education (Grant No. 2018R1A6A1A03024940). This work was also supported by Korea Environment Industry & Technology Institute (KEITI) through the Technology Development Project for Safety Management of Household Chemical Products Program, funded by Korea Ministry of Environment (MOE) (Grant No. 2020002960002).

[1] S. J. Singer and G. L. Nicolson, Science **175**, 720 (1972).
[2] K. Simons and E. Ikonen, Nature (London) **387**, 569 (1997).
[3] D. Lingwood and K. Simons, Science **327**, 46 (2010).
[4] K. Jacobson, O. G. Mouritsen, and R. G. W. Anderson, Nat. Cell Biol. **9**, 7 (2007).
[5] A. Parker, K. Miles, K. H. Cheng, and J. Huang, Biophys. J. **86**, 1532 (2004).
[6] W. F. D. Bennett, J.-E. Shea, and D. P. Tieleman, Biophys. J. **114**, 2595 (2018).
[7] M. Javanainen, H. Martinez-Seara, and I. Vattulainen, Sci. Rep. **7**, 1143 (2017).
[8] E. Drolle, W. F. D. Bennett, K. Hammond, E. Lyman, M. Karttunen, and Z. Leonenko, Soft Matter **13**, 355 (2017).
[9] G. A. Pantelopulos, T. Nagai, A. Bandara, A. Panahi, and J. E. Straub, J. Chem. Phys. **147**, 095101 (2017).
[10] E. Sezgin, I. Levental, S. Mayor, and C. Eggeling, Nat. Rev. Mol. Cell Biol. **18**, 361 (2017).
[11] D. Hakobyan and A. Heuer, PLoS ONE **9**, e87369 (2014).
[12] C. L. Armstrong, D. Marquardt, H. Dies, N. Kučerka, Z. Yamani, T. A. Harroun, J. Katsaras, A.-C. Shi, and M. C. Rheinstädter, PLoS ONE **8**, e66162 (2013).
[13] R. S. Davis, P. B. Sunil Kumar, M. M. Sperotto, and M. Laradji, J. Phys. Chem. B **117**, 4072 (2013).
[14] M. A. Barrett, S. Zheng, L. A. Toppozini, R. J. Alsop, H. Dies, A. Wang, N. Jago, M. Moore, and M. C. Rheinstädter, Soft Matter **9**, 9342 (2013).
[15] S. Baoukina, E. Mendez-Villuendas, W. F. D. Bennett, and D. P. Tieleman, Faraday Discuss. **161**, 63 (2013).
[16] Y. Oh and B. J. Sung, J. Phys. Chem. Lett. **9**, 6529 (2018).
[17] Y. Oh, E. S. Song, and B. J. Sung, J. Chem. Phys. **154**, 135101 (2021).
[18] F. Mollinedo and C. Gajate, Adv. Biol. Regul. **57**, 130 (2015).
[19] G. Vereb, J. Szöllosi, J. Matkó, P. Nagy, T. Farkas, L. Vigh, L. Mátyus, T. A. Waldmann, and S. Damjanovich, Proc. Natl. Acad. Sci. USA **100**, 8053 (2003).
[20] S. Thallmair, H. I. Ingólfsson, and S. J. Marrink, J. Phys. Chem. Lett. **9**, 5527 (2018).
[21] J. S. Goodwin, K. R. Drake, C. L. Remmert, and A. K. Kenworthy, Biophys. J. **89**, 1398 (2005).
[22] R. I. Kamar, L. E. Organ-Darling, and R. M. Raphael, Biophys. J. **103**, 1627 (2012).
[23] C. Arnarez, A. Webb, E. Rouvière, and E. Lyman, J. Phys. Chem. B **120**, 13086 (2016).
[24] R.-X. Gu, S. Baoukina, and D. P. Tieleman, J. Am. Chem. Soc. **142**, 2844 (2020).
[25] M. D. Weiner and G. W. Feigenson, J. Phys. Chem. B **123**, 3968 (2019).
[26] S. Meinhardt, R. L. C. Vink, and F. Schmid, Proc. Natl. Acad. Sci. USA **110**, 4476 (2013).
[27] S. J. Marrink, V. Corradi, P. C. T. Souza, H. I. Ingólfsson, D. P. Tieleman, and M. S. P. Sansom, Chem. Rev. **119**, 6184 (2019).
[28] H. J. Risselada and S. J. Marrink, Proc. Natl. Acad. Sci. USA **105**, 17367 (2008).
[29] W. F. D. Bennett, J. L. MacCallum, and D. P. Tieleman, J. Am. Chem. Soc. **131**, 1972 (2009).
[30] W. Kulig, H. Mikkolainen, A. Olzynska, P. Jurkiewicz, L. Cwiklik, M. Hof, I. Vattulainen, P. Jungwirth, and T. Róg, J. Phys. Chem. Lett. **9**, 1118 (2018).
[31] W. Kulig, L. Cwiklik, P. Jurkiewicz, and T. Róg, Chem. Phys. Lipids **199**, 144 (2016).
[32] A. Choubey, R. K. Kalia, N. Malmstadt, A. Nakano, and P. Vashishta, Biophys. J. **104**, 2429 (2013).
[33] S. Jo, H. Rui, J. B. Lim, J. B. Klauda, and W. Im, J. Phys. Chem. B **114**, 13342 (2010).
[34] Z. Zhang, L. Lu, and M. L. Berkowitz, J. Phys. Chem. B **112**, 3807 (2008).
[35] M. D. Weiner and G. W. Feigenson, J. Phys. Chem. B **122**, 8193 (2018).
[36] D. Marquardt, N. Kučerka, S. R. Wassall, T. A. Harroun, D. Bach, and J. Katsaras, Chem. Phys. Lipids **199**, 17 (2016).
[37] D. Marquardt, F. A. Heberle, D. V. Greathouse, R. E. Koeppe, R. F. Standaert, B. J. Van Oosten, T. A. Harroun, J. J. Kinnun, J. A. Williams, S. R. Wassall, and J. Katsaras, Soft Matter **12**, 9417 (2016).
[38] N. Kučerka, D. Marquardt, T. A. Harroun, M.-P. Nieh, S. R. Wassall, and J. Katsaras, J. Am. Chem. Soc. **131**, 16358 (2009).
[39] N. Kučerka, J. D. Perlmutter, J. Pan, S. Tristram-Nagle, J. Katsaras, and J. N. Sachs, Biophys. J. **95**, 2792 (2008).
[40] M. Javanainen and H. Martinez-Seara, Phys. Chem. Chem. Phys. **21**, 11660 (2019).
[41] T. Kwon, O.-S. Kwon, H.-J. Cha, and B. J. Sung, Sci. Rep. **9**, 16297 (2019).
[42] J. Jung, T. Kwon, Y. Oh, Y.-R. Lee, and B. J. Sung, J. Phys. Chem. B **123**, 9250 (2019).
[43] K.-I. Jo, Y. Oh, T.-H. Kim, J. Bang, G. Yuan, S. K. Satija, B. J. Sung, and J. Koo, ACS Macro Lett. **9**, 1483 (2020).
[44] G. A. Pantelopulos and J. E. Straub, Biophys. J. **115**, 2167 (2018).
[45] T. A. Wassenaar, H. I. Ingólfsson, R. A. Böckmann, D. P. Tieleman, and S. J. Marrink, J. Chem. Theory Comput. **11**, 2144 (2015).
[46] C. Arnarez, J. J. Uusitalo, M. F. Masman, H. I. Ingólfsson, D. H. De Jong, M. N. Melo, X. Periole, A. H. De Vries, and S. J. Marrink, J. Chem. Theory Comput. **11**, 260 (2015).

[47] S. J. Marrink and D. P. Tieleman, Chem. Soc. Rev. **42**, 6801 (2013).
[48] S. J. Marrink, H. J. Risselada, S. Yefimov, D. P. Tieleman, and A. H. de Vries, J. Phys. Chem. B **111**, 7812 (2007).
[49] S. J. Marrink, A. H. de Vries, and A. E. Mark, J. Phys. Chem. B **108**, 750 (2004).
[50] M. N. Melo, H. I. Ingólfsson, and S. J. Marrink, J. Chem. Phys. **143**, 243152 (2015).
[51] F.-G. Wu, H.-Y. Sun, Y. Zhou, G. Deng, and Z.-W. Yu, RSC Adv. **5**, 726 (2014).
[52] H. J. Berendsen, D. van der Spoel, and R. van Drunen, Comput. Phys. Commun. **91**, 43 (1995).
[53] D. Van Der Spoel, E. Lindahl, B. Hess, G. Groenhof, A. E. Mark, and H. J. C. Berendsen, J. Comput. Chem. **26**, 1701 (2005).
[54] M. J. Abraham, T. Murtola, R. Schulz, S. Páll, J. C. Smith, B. Hess, and E. Lindahl, SoftwareX **1–2**, 19 (2015).
[55] S. Kwon, S. Lee, H. W. Cho, J. Kim, J. S. Kim, and B. J. Sung, J. Chem. Phys. **150**, 204901 (2019).
[56] C. Bin Park, S. Kwon, and B. J. Sung, J. Chem. Phys. **151**, 054901 (2019).
[57] S. Kwon and B. J. Sung, Phys. Rev. E **102**, 022501 (2020).
[58] J.-H. Jeon, H. Martinez-Seara Monne, M. Javanainen, and R. Metzler, Phys. Rev. Lett. **109**, 188103 (2012).
[59] T. Akimoto, E. Yamamoto, K. Yasuoka, Y. Hirano, and M. Yasui, Phys. Rev. Lett. **107**, 178103 (2011).
[60] C. Hofsäß, E. Lindahl, and O. Edholm, Biophys. J. **84**, 2192 (2003).
[61] H. J. Berendsen, J. v. Postma, W. F. van Gunsteren, A. DiNola, and J. R. Haak, J. Chem. Phys. **81**, 3684 (1984).
[62] D. Marquardt, J. A. Williams, J. J. Kinnun, N. Kucerka, J. Atkinson, S. R. Wassall, J. Katsaras, and T. A. Harroun, J. Am. Chem. Soc. **136**, 203 (2014).
[63] D. Stelter and T. Keyes, J. Phys. Chem. B **121**, 5770 (2017).
[64] H. Park, C. B. Park, and B. J. Sung, Phys. Chem. Chem. Phys. **23**, 11980 (2021).
[65] C. B. Park and B. J. Sung, J. Phys. Chem. B **124**, 6894 (2020).
[66] H. Bae, Y.-H. Go, T. Kwon, B. J. Sung, and H.-J. Cha, Pharm. Res. **36**, 57 (2019).
[67] Y. Oh, J. Kim, A. Yethiraj, and B. J. Sung, Phys. Rev. E **93**, 012409 (2016).
[68] G. Kwon, B. J. Sung, and A. Yethiraj, J. Phys. Chem. B **118**, 8128 (2014).
[69] M. R. Vist and J. H. Davis, Biochemistry **29**, 451 (1990).
[70] K. Suga and H. Umakoshi, Langmuir **29**, 4830 (2013).
[71] R.-X. Gu, S. Baoukina, and D. P. Tieleman, J. Chem. Theory Comput. **15**, 2064 (2019).
[72] S. L. Veatch and S. L. Keller, Biophys. J. **85**, 3074 (2003).
[73] S. L. Veatch and S. L. Keller, Phys. Rev. Lett. **94**, 148101 (2005).
[74] T. A. Harroun, J. Katsaras, and S. R. Wassall, Biochemistry **47**, 7090 (2008).
[75] S. J. Marrink, A. H. de Vries, T. A. Harroun, J. Katsaras, and S. R. Wassall, J. Am. Chem. Soc. **130**, 10 (2008).
[76] T. Kwon and B. J. Sung, Phys. Rev. E **102**, 052501 (2020).
[77] H. Im, Y. Oh, H. W. Cho, J. Kim, K. Paeng, and B. J. Sung, Soft Matter **309**, 456 (2017).
[78] T. P. Trouard, A. A. Nevzorov, T. M. Alam, C. Job, J. Zajicek, and M. F. Brown, J. Chem. Phys. **110**, 8802 (1999).
[79] A. Filippov, G. Orädd, and G. Lindblom, Biophys. J. **84**, 3079 (2003).
[80] C. L. Armstrong, M. A. Barrett, A. Hiess, T. Salditt, J. Katsaras, A.-C. Shi, and M. C. Rheinstädter, Eur. Biophys. J. **41**, 901 (2012).
[81] T. A. Harroun, J. Katsaras, and S. R. Wassall, Biochemistry **45**, 1227 (2006).